

# ENHANCED REFRACTIVE INDEX SENSOR BASED ON ETCHED CORELESS FIBER

Noor Hamza<sup>1</sup>, hanan tahar<sup>1</sup>, and saif mohammed<sup>1</sup>

<sup>1</sup>Institute of laser for postgraduate studies

May 5, 2020

## Abstract

A high sensitivity refractive index (RI) sensor based on a multimode interference arises from the self-imaging effect in single-mode–multimode–single-mode fiber structure was experimentally demonstrated. The sensor performance with different coreless fiber diameter (CLF) was examined to obtain an appropriate dimension of extreme evanescent fields. Various diameters of CLF of 100 and 50  $\mu\text{m}$  with three different tune lengths 20, 25 and 30 mm were achieved by chemical etching technique based on hydrofluoric (HF) acid plunging. The sensor performance is recognized by determining the spectral shift from the transmission spectrum for different values of refractive indices. The highest sensor sensitivity of about 1012 nm/RIU was attained when the CLF diameter was 50  $\mu\text{m}$ . This sensor offers an appropriate and economical technique for applications of RI measurement.

## 1. INTRODUCTION

All-optical fiber based-sensors, due to their intrinsic characteristic of simple, compact size, cost-effective, resistance to electromagnetic interference, good hostility to corrosion, durability, flexibility, accuracy and so on [1] have interested considerable attention in many applications such as medical applications [2–4], chemical [5], and environmental [6]. They have been effectively applied as refractive index (RI) [7,8], temperature [9], displacement [10], environmental monitoring [11], humidity [12,13], strain [14], acoustic [15], force [16] sensors and so on. Optical fiber based-refractive-index (RI) sensors or refractometers are actually beneficial in a diversity of industrial applications like chemical or biological sensors [8]. In comparison to conventional refractive index sensors like optical path measurement method, Optical fiber based-RI sensors have drawn distinct concentration owing to the compact size, high sensitivity and the appropriateness for remote sensing [17,18].

To date, a series of RI sensors have been fabricated based on the long-period fiber grating (LPFG) [19], fiber Bragg grating (FBG) [20], Fabry-Perot interferometer (FPI) [12], Mach-Zehnder interferometer (MZI) [21], photonic crystal fiber (PCF) [1], and single-mode fiber-coreless fiber-single mode fiber (SCS) [22].

But, most of these fiber structures are exposed to damage that causes the fabrication process more complex and costly. Single-mode–multimode–single-mode (SMS) fiber configuration which is usually constructed by splicing a multimode fiber (MMF) or PCF section between two single-mode fiber (SMF) section [1,23,24]. The conventional method to enhance the sensitivity of an in-line MZI sensor is by enlarging its cavity length [20]. However, the long cavity leads to more difficult to package the sensor. Herein, CLF which is operational analogous to MMF has won more attraction of RI sensing application, in which the sensitivity can be improved by reducing the diameter of the CLF [12]. The RI-SCS configuration depends on the principle of multimode interference (MMI). As the core mode of the propagated in single-mode fiber section, a number of high-order modes are excited and guided through the CLF. Then, at the other splicing point, the high-order modes are coupled and backward to the core fiber of the single-mode fiber [25]. Additionally, when the light passes via the CLF which functions as the sensing area, the evanescent wave absorption

varies with the variation in the surrounding environmental medium. This causes to the varies into the RI of the outer medium (which acts as a cladding layer) and subsequently the output transmission signal will be modified [26].

In this work, the RI sensing structure comprises of single-mode fiber-coreless fiber-single mode fiber (SCS) configuration and the encirclement refractive index behaves as the cladding of the CLF. The sensor performance of SCS configuration with different CLF diameters and lengths has been investigated. The CLF diameter is decreased by the chemical etching method. The better sensor sensitivity was attained when the CLF diameter was 50  $\mu\text{m}$ .

## SENSING PRINCIPLE

The SCS sensor structure comprises of two segment of single-mode fiber (SMF) and one segment of CLS in between. The three segment are spliced together. The schematic diagram of the SCS sensor configuration is depicted in the Fig.1 (A-B). As the light injected into the first section of SMF, the redoubled high-order linear polarization (LP) modes have been excited. Then the light travels through SMF-CLF at the first splicing point, high-order modes will be propagated via the CLF with diverse propagation constants. After that, as the light propagated through the second splicing point of CLF-SMF, these modes will be reconnected to create the modal interference. Consequently, the characteristic of the output spectrum is varied with contrast to the input spectrum. The modal field shapes for these modes (normalized with regard to the all cross-section of the fiber) can excellently be estimated by that of an infinitely total parabolic media.

For a standard multi-mode fiber including CLF, the propagation constants of the  $m$  and  $n$  symmetric modes can be given as [23]:

$$\beta_m - \beta_n = \frac{u_m^2}{2k_0 a^2} - \frac{u_n^2}{2n_{\text{core}}^2} \quad (1)$$

Where  $\beta_m$  and  $\beta_n$  are the longitudinal propagation constants for the order modes  $m$ ,  $n$ .  $u_m$  and  $u_n$  are the normalized transverse propagation constants, while the  $a$  is the core radius of the CF,  $n_{\text{core}}$  is the core refractive index of the CF.

As the phase difference between the two modes is the integer multiple of  $2\pi$ , constructive interference can occur in condition:

$$(\beta_m - \beta_n)L = 2\pi N \quad (2)$$

Then, the wavelength of the constructive interference can be given as [23]:

$$\lambda = \frac{8(2N+1)n_{\text{core}} a^2}{(m+n)[2(m+n)-1]L} \quad (3)$$

where the  $L$  is the CLF length and  $N$  is the natural number.

While, the wavelength difference is [23]:

$$\Delta\lambda = \lambda_N - \lambda_{N-1} = \frac{16 n_{\text{core}} a^2}{(m-n)[2(m+n)-1]L} \quad (4)$$

From these relations, it worthy known that the dips and peaks are related to  $L$  which peaks have the tendency to be intensive as  $L$  varied. The boundary condition for the light propagated in the CLF is altered when the surrounding RI is changed. The mode field and propagation constant are fixed. From equation (2), the phase condition of the destructive or constructive interference is varied and  $N$  is also varied as the propagation constants are altered. Moreover, it can be observed that the constructive or destructive interference wavelength shift. The wavelength shift variations depend on the changing values of the surrounding RI [23].

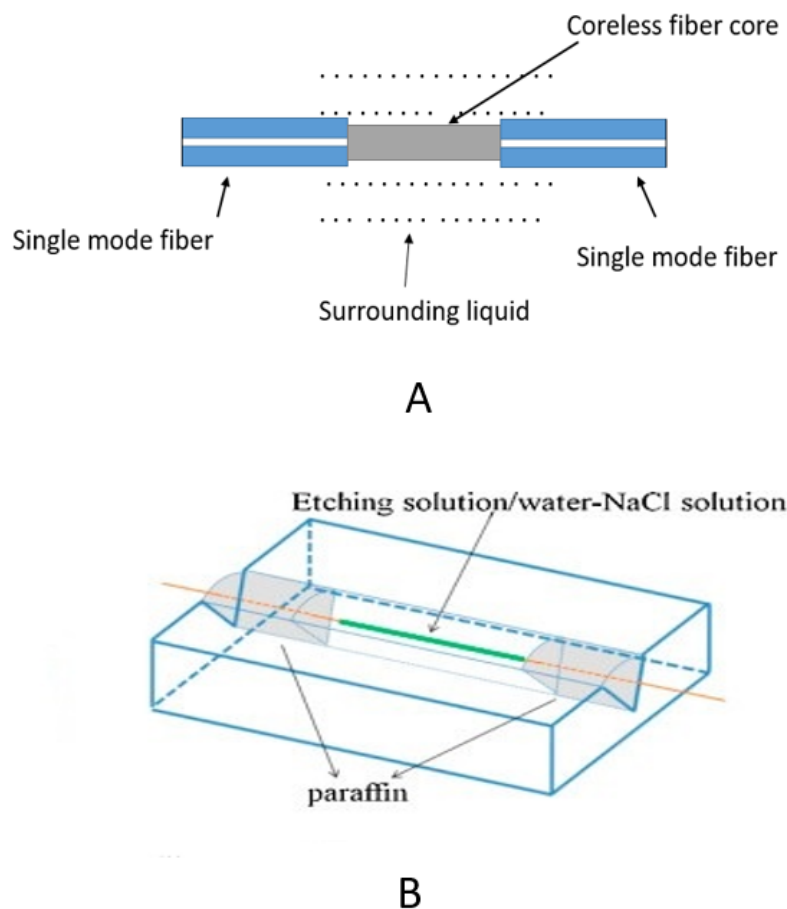


Fig. (1): The schematic diagram of sensor structure: (A) SMS fiber structure, (B) The V shape groove with fiber structure on it.

### Sensor structure fabrication:

The SCS configuration based refractive index sensor is display Figure (2). the sensor structure comprises of a broadband source (BBS Thorlabs S5FC10055) with a wavelength range of 1400 nm to 1600 nm), two segments of SMF (Coring SMF-28) and one Segment of CLS (FG125LA from Thorlabs) in between. BBS was connected to the SMF-CLF-SMF (SCS) structure from the first section of SMF and the other end of this structure connected to an optical spectrum analyzer (OSA YOKOGAWA AQ6370C) to detect the response transmission spectrum of the RI sensor. Where SMF spliced to CLF (three different lengths) by fusion splicer (Fujikura FSM-60S), the interference between the fundamental mode and the higher-order modes happens in a second spliced area between the CLF and SMF. To examine RI sensor response, The SCS configuration submerged in U groove which contains the NaCl solution with different concentrations.

RI sensor was studied for three different lengths with 20, 25 and 30 mm of CLF which is represented the sensing area. Since the CLF diameter is an essential factor in SCS fiber configuration to attain extreme sensitivity, the effect of CLF diameter on the RI sensing sensitivity was investigated. Accordingly, various tuned diameters of CLF of 100, 75 and 50  $\mu\text{m}$  were achieved for each length. The CLF diameter was chemically etched using 40% hydrofluoric (HF) acid immersion. The construction method of SCS fiber

configuration began with stripped-off the acrylate coating from CLF and SMF, then the CLF fusion spliced from both ends with SMF. Then, the fabricated SCS construction was set in a U-shaped groove. This groove was utilized to include the etching liquid acid (HF 40%). The 100, 75 and 50  $\mu\text{m}$  CLF diameter was realized by controlling the etching time. The etching method was retained in CLF section, and the splicing zone was verified under the microscope in each single case to make certain that no etching happened due to HF liquid.

The sodium chloride solution (NaCl) was utilized as a testing solution, which was prepared by dissolving NaCl in 100 ml of deionized water utilizing the magnetic stirrer at room temperature (25°C). Under a controlled laboratory environment, a group of solutions had been made from different concentrations of NaCl powder (0, 5, 10, 15, 20 and 25 %) of NaCl dissolved in deionized water. The concentration corresponding to different RIs of 1.333-1.382 ranges. Abbe refractometer was utilized to measure the RI of the solution. In our experiment, the sensing area of the structure is totally submerged in these solutions and before each single measurement, the structure is cleaning by the deionized water and dried in air.

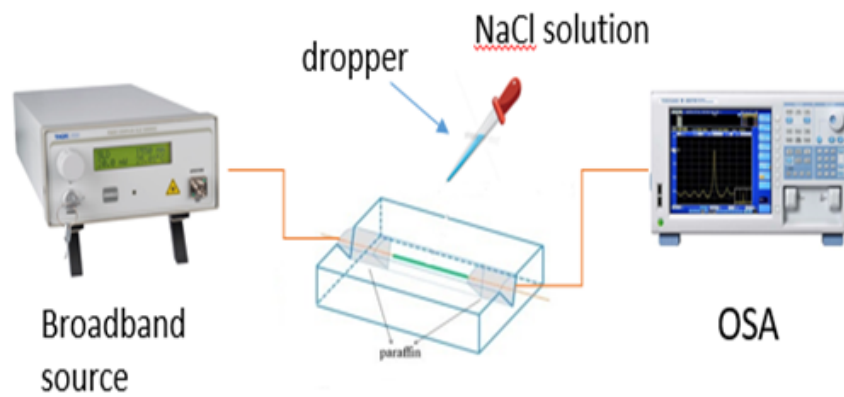
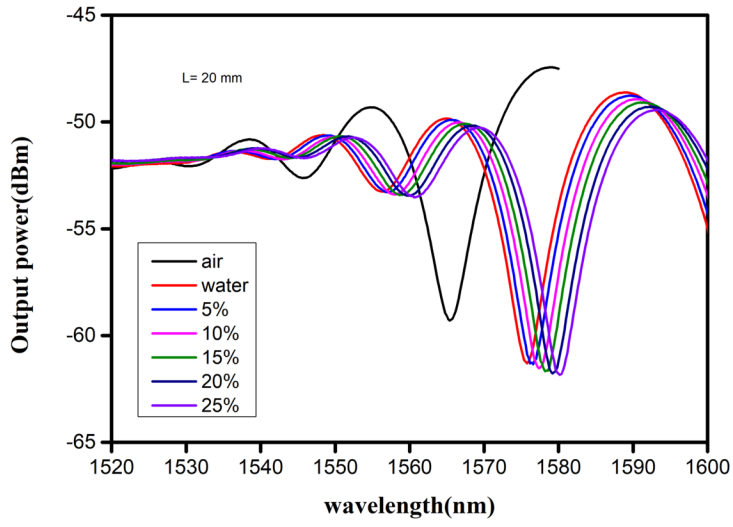


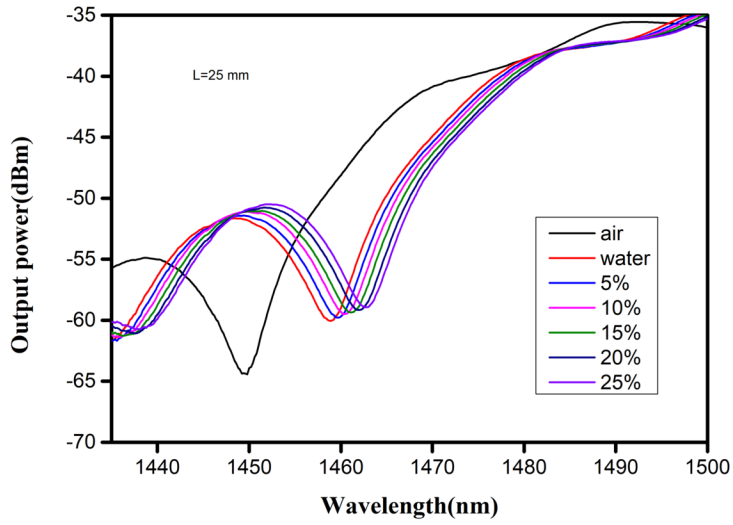
Fig. (2): The RI sensor system.

## Result and discussion

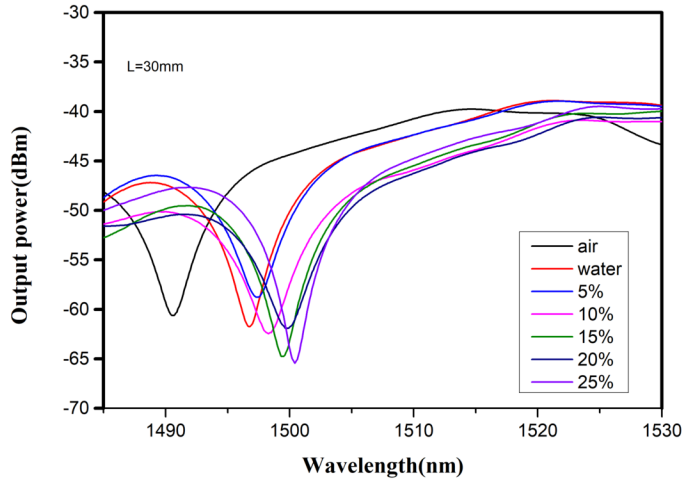
The experimental setup is displayed in Fig. 2. Firstly, the response of the fundamental SCS fiber configuration with 125  $\mu\text{m}$  diameter of CLF (i.e. without etching) towards the in air determined which revealed a reasonably good extinction ratio, as shown in Fig. 3(A-C). Then, RI sensitivity of the assembled SCS configuration was investigated by immersing the sensor to various concentrations of NaCl solution corresponding to different RIs in range of 1.333-1.382 to investigate the surrounding RI response of SCS, while the temperature was preserved at the room temperature (25°C).



A



B



C

Fig. (3): The transmission spectra of 125 $\mu$ m diameter for (A): length 20 mm, (B): length 25 mm and (C): length 30 mm.

The transmission spectra response of the designed RI fiber sensor for different sensing length of about 20, 25 and 30 mm is depicted in Fig.3 (A-C). The stimulated evanescent signals will interact with the surrounding RI and initiate the variation in output spectrum. Besides from this Figure, it can be observed that when the RI rises the transmission spectra shifted to longer wavelength. The RI rises from 1.333-1.382, the wavelength was shifted from 1565.5 nm to 1580.4, 1449 nm to 1462.7 and 1562.6 nm to 1578 for lengths 20, 25 and 30 mm respectively. The sensitivities of the fundamental SCS fiber configuration with different CLF lengths (without etching) based RI fiber sensor can be illustrated in table 1, 2 and 3. This is owing to the actuality that, when the light propagates from SMF to CLF, the higher order modes would be agitated and interfered through the CLF length payable to the effect of MMI. Then, as the RI rises, the surrounding medium which function as the cladding layer of the sensing area will be influence by outer solution.

Table 1: The sensitivities of RI sensor with CLF diameter of 125  $\mu$ m and length of 20 mm.

Refractive index	Wavelength shift (nm)	Sensitivity (nm/RIU)
1.33	17.5	350
1.34	21.2	424
1.35	22.3	446
1.36	24.1	482
1.37	26.1	522
1.38	27.6	552

Table 2: The sensitivities of RI sensor with CLF diameter of 125  $\mu$ m and length of 25 mm.

Refractive index	Wavelength shift (nm)	Sensitivity (nm/RIU)
1.33	17.5	350
1.34	21.2	424

Refractive index	Wavelength shift (nm)	Sensitivity (nm/RIU)
1.35	22.3	446
1.36	24.1	482
1.37	26.1	522
1.38	27.6	552

Table 3: The sensitivities of RI sensor with CLF diameter of 125  $\mu\text{m}$  and length of 30 mm.

Refractive index	Wavelength shift (nm)	Sensitivity (nm/RIU)
1.33	6.7	134
1.34	6.9	138
1.35	7.8	156
1.36	9.1	182
1.37	9.3	186
1.38	9.8	196

The wavelength shifts versus surrounding RI for various lengths of the CLF segment are depicted in figure 5. It is clear that decreasing the CLF diameters have influenced on multimode interference and display a larger wavelength shift resulted in a higher sensitivity of the RI sensor.

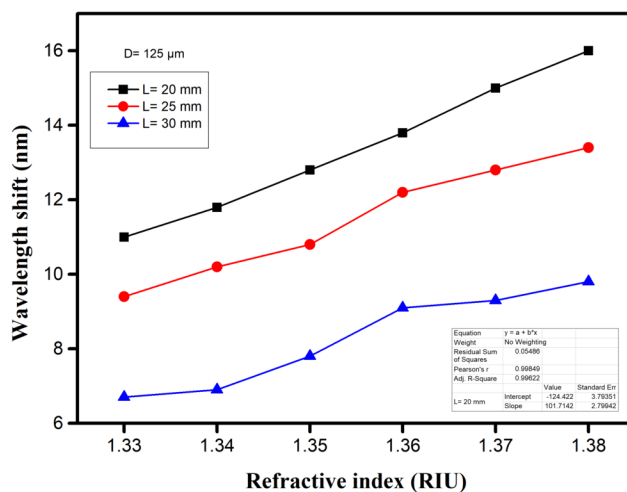


Fig 5. The wavelength shift versus the surrounding RI for fixed diameter.

For the etched CLF with a diameter of 100  $\mu\text{m}$  and a tuned length of 20, 25 and 30 mm, the calculated sensitivities listed in table 4, 5 and 6 for varies refractive indices. From these results, it can be notice that the sensing length of 25 mm has the highest sensitivity.

Table 4: The sensitivities of RI sensor with CLF diameter of 100  $\mu\text{m}$  and length of 20 mm.

Refractive index	Wavelength shift (nm)	Sensitivity (nm/RIU)
1.33	17.5	350
1.34	21.2	424
1.35	22.3	446
1.36	24.1	482
1.37	26.1	522
1.38	27.6	552

Table 5: The sensitivities of RI sensor with CLF diameter of 100  $\mu\text{m}$  and length of 25 mm.

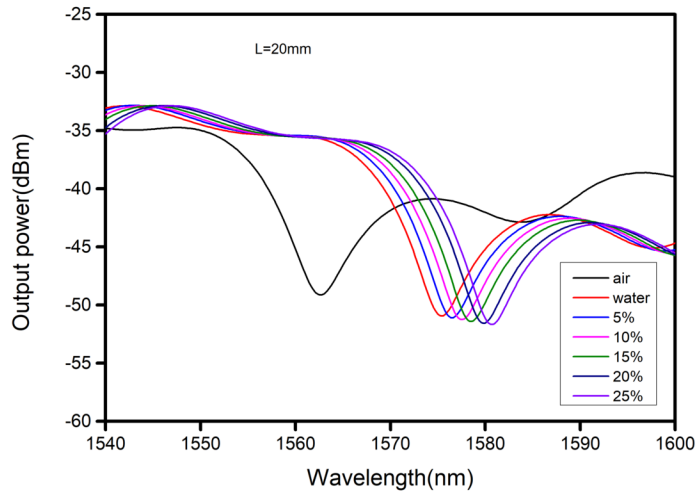
Refractive index	Wavelength shift (nm)	Sensitivity (nm/RIU)
1.33	17.5	350
1.34	21.2	424
1.35	22.3	446
1.36	24.1	482
1.37	26.1	522
1.38	27.6	552

Table 6: The sensitivities of RI sensor with CLF diameter of 100  $\mu\text{m}$  and length of 30 mm.

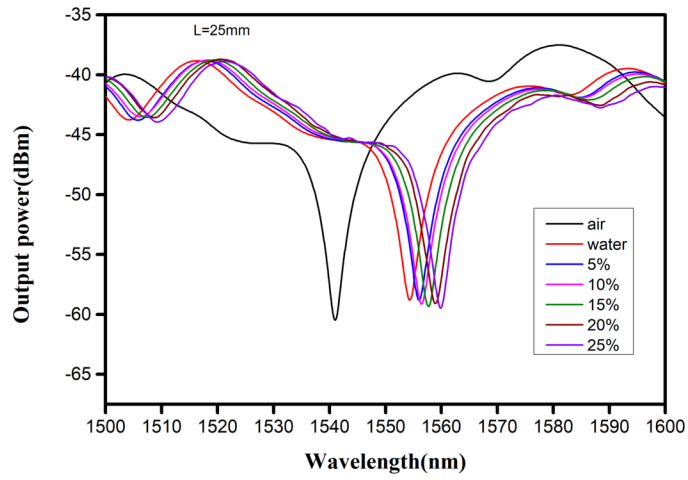
Refractive index	Wavelength shift (nm)	Sensitivity (nm/RIU)
1.33	17.5	350
1.34	21.2	424
1.35	22.3	446
1.36	24.1	482
1.37	26.1	522
1.38	27.6	552

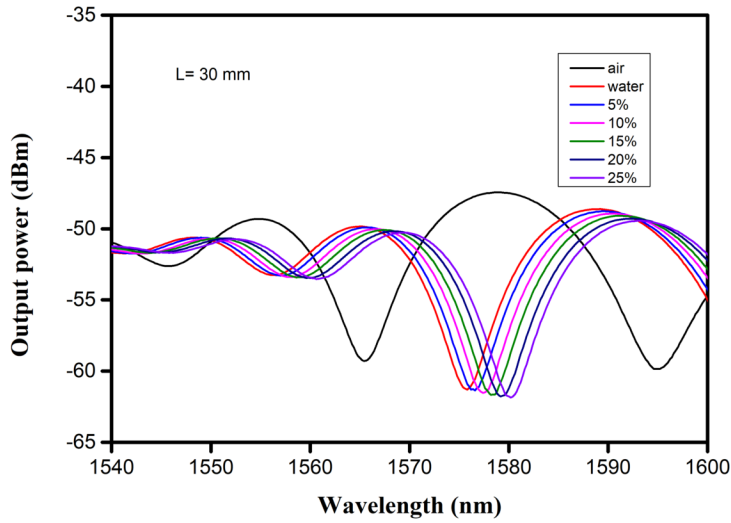
Figure 6(A-C) represent the transmission response for the etched CLF of a diameter of 100  $\mu\text{m}$  with various tuned lengths 20, 25 and 30 mm.

A



B





C

Fig. (6): The transmission spectra of 100µm diameter for (A): length 20 mm, (B): length 25 mm and (C): length 30 mm.

Figure 7 explains the relationship between RI and the wavelength shift which the spectral shift rises by reducing the diameter for three CLF lengths.

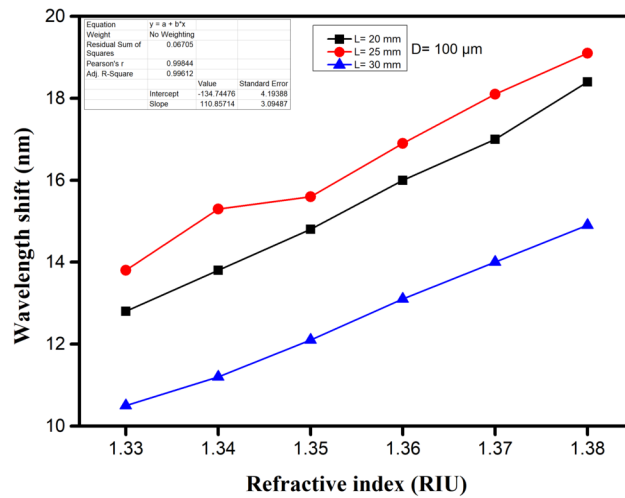
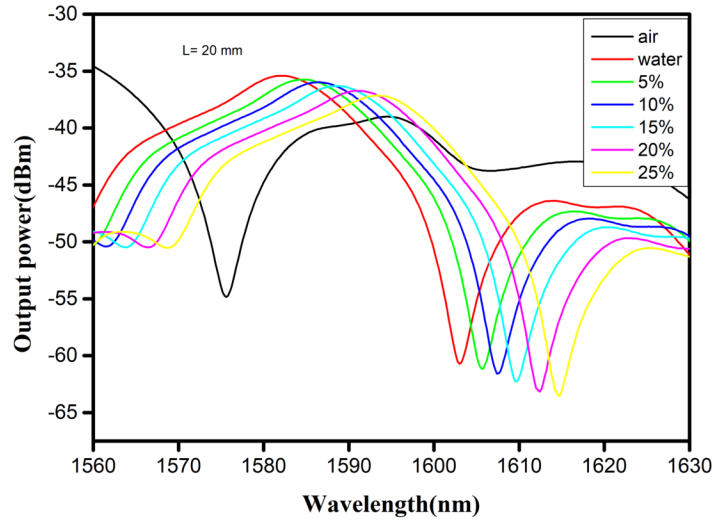


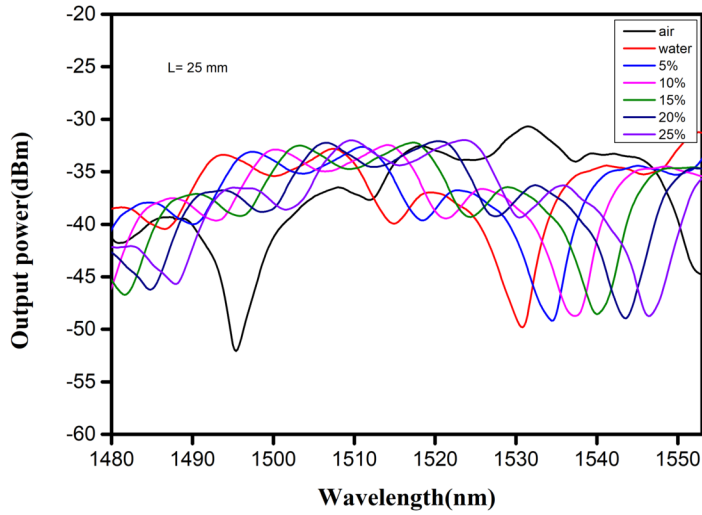
Fig 7. The wavelength shift versus the surrounding RI for fixed diameter.

Figure 8 (A-C) displays the spectral shifts of the proposed RI fiber sensor with CLF diameter of 50 µm and varies lengths against various RI values. These results confirm that the RI sensitivity is improved by

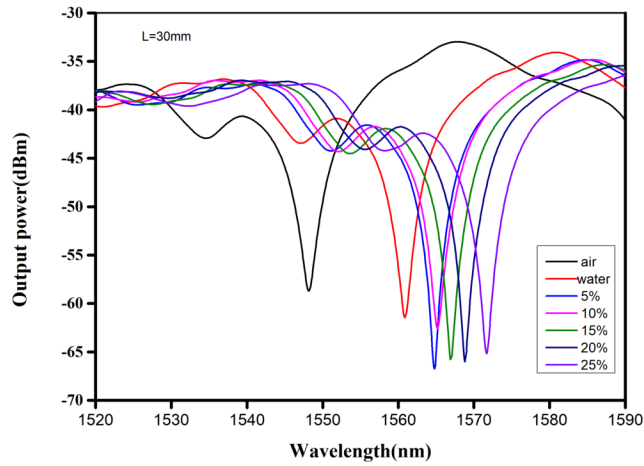
decreasing the diameter of the CLF. The calculated sensitivities were arranged in table 7, 8 and 9 for length of 20, 25 and 30 mm respectively.



A



B



C

Fig. (8): The transmission spectra of 50 $\mu$ m diameter for (A): length 20 mm, (B): length 25 mm and (C): length 30 mm.

Table 6: The sensitivities of RI sensor with CLF diameter of 50  $\mu$ m and length of 20 mm.

Refractive index	Wavelength shift (nm)	Sensitivity (nm/RIU)
1.33	17.5	350
1.34	21.2	424
1.35	22.3	446
1.36	24.1	482
1.37	26.1	522
1.38	27.6	552

Table 8: The sensitivities of RI sensor with CLF diameter of 50  $\mu$ m and length of 25 mm.

Refractive index	Wavelength shift (nm)	Sensitivity (nm/RIU)
1.33	17.5	350
1.34	21.2	424
1.35	22.3	446
1.36	24.1	482
1.37	26.1	522
1.38	27.6	552

Table 9: The sensitivities of RI sensor with CLF diameter of 50  $\mu$ m and length of 30 mm.

Refractive index	Wavelength shift (nm)	Sensitivity (nm/RIU)
1.33	17.5	350

Refractive index	Wavelength shift (nm)	Sensitivity (nm/RIU)
1.34	21.2	424
1.35	22.3	446
1.36	24.1	482
1.37	26.1	522
1.38	27.6	552

From these results, it can be observed that the greatest RI sensitivity of the proposed configuration was with CLF of 50  $\mu\text{m}$  diameter and 25 mm length. It represents the minimum portion of the light transmitting via the fiber that induces highest evanescent fields, causing in an improvement of optical interaction between the surrounding RI light and the fiber-guided. Corresponding to MMI principle, the length and diameter of CLF would influence the output spectra and too there is an optimum length for every diameter to preserve the self-imaging and reduction the losses. As illustrated in figure 9 the linear fitting coefficient ( $R^2$ ) is 0.998 for SCS fiber configuration with 50  $\mu\text{m}$  diameter and 25 mm length, which exhibits an excellent RI sensing features of the SCS-based sensor.

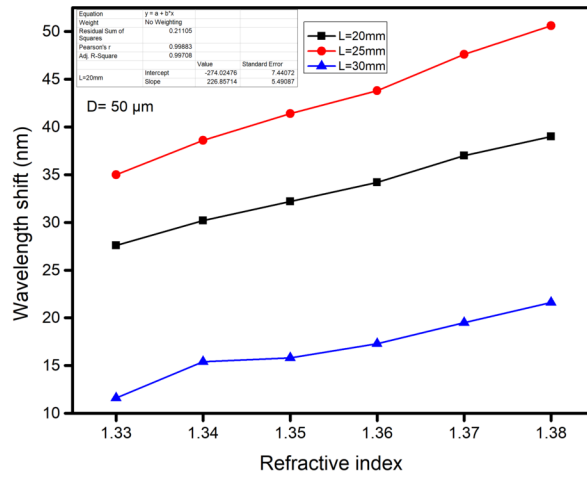


Fig.9: The wavelength shift versus the surrounding RI for CLF diameter of 50  $\mu\text{m}$ .

Additionally, it can be observed that the transmission response of the proposed SCS sensor reveals a significant red-shift, this due to the lower refractive indices of the surrounding material which the surrounding ambient function as a cladding layer.

A recently published work utilizing various fiber configurations, as presented in Table 10. The spectral sensitivity of the current SCS sensor larger sensitivity and good performance in compare to other work.

Table 10: comparison between the sensitivities of this work and other researchers.

researcher	Sensor structure	Diameter ( $\mu\text{m}$ )	Refractive index range	Sensitivity (nm/RIU)	Reference
Yong Zhao et al.	SMF-MMF-SMF	40	1.33- 1.4	286.2	[17]

researcher	Sensor structure	Diameter ( $\mu\text{m}$ )	Refractive index range	Sensitivity (nm/RIU)	Reference
Min shao et al.	SMF-TF-MMF-SMF	90	1.33- 1.42	148.27	[19]
Haifeng DU et al.	SMF-PCF-SMF	112 91	1.33- 1.38 1.33- 1.38	211.53 359.37	[7] [7]
Saif A. et al.	SMF-CF-SMF	60	1.33- 1.38	340.85	[20]
This work	SMF-CLF-SMF	100 50	1.33- 1.38 1.33- 1.38	382 1012	

## CONCLUSION

In this paper, an all-optical fiber RI sensor based on multimode interference has been proposed and experimentally demonstrated. SCS configuration comprises of CLF section which represent the sensing area spliced between two small pieces of SMF. A various diameters of CLF of 100 and 50  $\mu\text{m}$  with three different tune lengths 20, 25 and 30 mm have been employed as a sensing area to substitute the traditional MMF. The effect of CLF diameter variation on the sensor performance has been examined. Chemical etching process was used to tune the CLF diameter from 100 to 50  $\mu\text{m}$ . The experimental results of the SCS configuration encompassed of the etched CLF at 50  $\mu\text{m}$  diameter with a CLF length of 25 mm exhibited the greatest sensitivity of about 1012 nm/RIU. The SCS structure has attractive benefits such as low cost, high measurement sensitivity, simple structure, and fast response.

## CONFLICT OF INTEREST

The authors declare that there is no conflict of interest that could be perceived as prejudicing the impartiality of the research reported.

## REFERENCE

1. H. Du, X. Sun, Y. Hu, X. Dong, and J. Zhou, "High Sensitive Refractive Index Sensor Based on Cladding Etched Photonic Crystal Fiber Mach-Zehnder Interferometer," *Photonic Sensors* **9** , 126–134 (2019).
2. A. Vaz, N. Barroca, M. Ribeiro, A. Pereira, and O. Frazão, "Optical Fiber Humidity Sensor Based on Polyvinylidene Fluoride Fabry–Perot," *IEEE Photonics Technology Letters* **31** , 549–552 (2019).
3. S. Zheng, Y. Zhu, and S. Krishnaswamy, "Nanofilm-coated long-period fiber grating humidity sensors for corrosion detection in structural health monitoring," in *Proc.SPIE* (2011), Vol. 7983.
4. Y. Zhao, M. Lei, S.-X. Liu, and Q. Zhao, "Smart hydrogel-based optical fiber SPR sensor for pH measurements," *Sensors and Actuators B: Chemical* **261** , 226–232 (2018).
5. L. Zhao, L. Jiang, S. Wang, H. Xiao, Y. Lu, and H.-L. Tsai, "A High-Quality Mach-Zehnder Interferometer Fiber Sensor by Femtosecond Laser One-Step Processing," *Sensors* **11** , (2011).
6. M. Kraft, M. Jakusch, M. Karlowatz, A. Katzir, and B. Mizaikoff, "New Frontiers for Mid-Infrared Sensors: Towards Deep Sea Monitoring with a Submarine FT-IR Sensor System," *Applied Spectroscopy* **57** , 591–599 (2003).
7. B. Yang, Y. Niu, B. Yang, Y. Hu, L. Dai, Y. Yin, and M. Ding, "High sensitivity balloon-like refractometric sensor based on singlemode-tapered multimode-singlemode fiber," *Sensors and Actuators A: Physical* **281** , 42–47 (2018).
8. W. Yang, S. Zhang, T. Geng, L. Li, G. Li, Y. Gong, K. Zhang, C. Tong, C. Lu, W. Sun, and L. Yuan, "High Sensitivity Refractometer Based on a Tapered-Single Mode-No Core-Single Mode Fiber Structure," *Sensors* **19** , (2019).

9. K. Tian, G. Farrell, E. Lewis, X. Wang, H. Liang, and P. Wang, "A high sensitivity temperature sensor based on balloon-shaped bent SMF structure with its original polymer coating," *Measurement Science and Technology* **29** , 85104 (2018).
10. R. C. Spooncer, C. Butler, and B. E. Jones, "Optical fiber displacement sensors for process and manufacturing applications," *Optical Engineering* **31** , 1632–1637 (1992).
11. A. Lay-Ekuakille, G. Griffo, S. Maggi, G. Passarella, and E. Barca, "Environmental Monitoring of Sea: Optical Fiber Sensor Design," in *6th EnvImeko-Imeko TC19* (2016).
12. H. Alswefe, S. K. Al-Hayali, and A. H. M. Al-Janabi, "Efficient humidity sensor based on an etched no-core fiber coated with copper oxide nanoparticles," *Journal of Nanophotonics* **12** , 1–12 (2018).
13. H. Y. Zebian and H. J. Taher, "Relative humidity sensor based on no-core multimode interferometer coated with Al<sub>2</sub>O<sub>3</sub>-PVA composite films," *Optical Fiber Technology* **54** , 102110 (2020).
14. X. Zhong, Y. Wang, J. Qu, C. Liao, S. Liu, J. Tang, Q. Wang, J. Zhao, K. Yang, and Z. Li, "High-sensitivity strain sensor based on inflated long period fiber grating," *Optics Letters* **39** , 5463–5466 (2014).
15. J. Ma, W. Jin, H. Xuan, C. Wang, and H. L. Ho, "Fiber-optic ferrule-top nanomechanical resonator with multilayer graphene film," *Optics Letters* **39** , 4769–4772 (2014).
16. Y. Wu, S. Xiao, Y. Xu, Y. Shen, Y. Jiang, W. Jin, Y. Yang, and S. Jian, "Highly sensitive force sensor based on balloon-like interferometer," *Optics & Laser Technology* **103** , 17–21 (2018).
17. K. Tian, G. Farrell, X. Wang, E. Lewis, and P. Wang, "Highly sensitive displacement sensor based on composite interference established within a balloon-shaped bent multimode fiber structure," *Applied Optics* **57** , 9662–9668 (2018).
18. M. Y. M. Noor, A. I. Azmi, A. S. Abdullah, A. S. M. Supa'at, N. M. Kassim, M. H. Ibrahim, and N. H. Ngajikin, "High Sensitivity of Balloon-Like Bent MMI Fiber Low-Temperature Sensor," *IEEE Photonics Technology Letters* **27** , 1989–1992 (2015).
19. F. Zou, Y. Liu, C. Deng, Y. Dong, S. Zhu, and T. Wang, "Refractive index sensitivity of nano-film coated long-period fiber gratings," *Optics Express* **23** , 1114–1124 (2015).
20. W. Liang, Y. Huang, Y. Xu, R. K. Lee, and A. Yariv, "Highly sensitive fiber Bragg grating refractive index sensors," *Applied Physics Letters* **86** , 151122 (2005).
21. X.-Y. Sun, D.-K. Chu, X.-R. Dong, Chu-Zhou, H.-T. Li, Luo-Zhi, Y.-W. Hu, J.-Y. Zhou, Cong-Wang, and J.-A. Duan, "Highly sensitive refractive index fiber inline Mach-Zehnder interferometer fabricated by femtosecond laser micromachining and chemical etching," *Optics & Laser Technology* **77** , 11–15 (2016).
22. Y. Li, Z. Liu, and S. Jian, "Multimode interference refractive index sensor based on coreless fiber," *Photonic Sensors* **4** , 21–27 (2014).
23. Y. Zhao, L. Cai, X.-G. Li, F. Meng, and Z. Zhao, "Investigation of the high sensitivity RI sensor based on SMS fiber structure," *Sensors and Actuators A: Physical* **205** , 186–190 (2014).
24. & A. H. A.-J. S.A. Mohammed, "All Fiber Chemical Liquids Refractive Index Sensor Based on Multimode Interference," *Iraqi Journal of Laser* **17** , 33–39 (2018).
25. M. Shao, X. Qiao, H. Fu, H. Li, Z. Jia, and H. Zhou, "Refractive Index Sensing of SMS Fiber Structure Based Mach-Zehnder Interferometer," *IEEE Photonics Technology Letters* **26** , 437–439 (2014).
26. W. A. Khaleel and A. H. M. Al-Janabi, "High-sensitivity sucrose erbium-doped fiber ring laser sensor," *Optical Engineering* **56** , 1–7 (2017).